Front. Chem. China 2010, 5(3): 262–276
DOI 10.1007/s11458-010-0211-8

FEATURE ARTICLE

The crystallization and morphology of melt-miscible polymer blends

Jerold M. SCHULTZ (✉)

Department of Chemical Engineering, University of Delaware, Newark, DE 19711, U.S.A.

The morphology and kinetics of crystallization from melt-miscible blends is reviewed for binary systems in which either one or both polymer components are crystallizable. In systems in which one component (component A) crystallizes first, the other component (B) may reside finally between spherulites, between growth arms (composed of a stack of A crystalline lamellae), or between crystal lamellae of A. The kinetics of component redistribution dictates which site must become primary. It is shown that the diffusivity D of the components in the melt and the velocity V of spherulite growth combine through the diffusion length $\delta = D/V$ to define the final location for component B and to also define whether spherulite propagation will be linear or parabolic in time. When crystallization of both components proceeds concurrently, by forming spherulites of A and of B, the spherulites are prone to interpenetrate or to form concentric spherulites. Cooperative crystallization, in which the kinetics of a rapidly crystallizing component and a slowly crystallizing component are both affected such that the two crystallize nearly simultaneously, is discussed. Finally, the competition between liquid-liquid phase separation and crystallization in systems with either an upper or lower critical solution temperature is reviewed.

Keywords blends, crystallization, morphology

1 Introduction

A convenient way to control or alter the properties of materials systems is to mix two or more components together, forming a product whose behavior is different in useful ways from that of the components. For small-molecule systems, the mixing may be within individual crystals or within a glass, or it may be at a higher level, between microscopic crystals of different compositions. For small-molecule systems in the solid state, for instance metal alloys, the components can be intimately mixed within the same crystal, since the small size of the molecules (or individual atoms) allows the energy of the geometrical or chemical mismatch between molecules to be confined to a very small volume. For polymers, however, with strong covalent bonding extending linearly over enormous distances along polymer chains, the effect of a local mismatch is propagated through the crystal, creating a large increase in the internal energy of the crystal. For this reason, intimate mixing within a crystal (cocrystallization) is precluded, except for systems with nearly identical repeat units along the chain. Therefore, the final state of a useful solid polymer blend would be as intimately mixed crystals of the components.

Since useful polymer products are usually formed by solidification from the melt, we will focus our attention here on blends solidified from the homogeneous melt. Further, since neat polymer systems – and polymer blends – nearly always organize as spherulites when crystallized from the melt, our attention is further focused on the state of spherulitic aggregation. We shall see that a wide range of morphological possibilities exists, ranging from separate spherulites of the component polymers to nanoscale intercalation.

We shall further see that whichever morphological state develops during solidification depends largely on the kinetics of transport of the components to and from a growing crystalline body. These conditions, as we shall see, can be described in terms of a diffusion length.

This review is organized as follows. We will first examine the range of morphological possibilities available to binary

Received February 3, 2010; accepted March 29, 2010
E-mail: schultz@udel.edu

polymer blends of fully melt-miscible polymers, of which one or both components are crystallizable. We will then examine the kinetics of solidification, including, especially, the mass transport near the growth front. We will finally look at systems in which liquid-liquid phase separation competes with crystallization.

During the review of this paper, attention was called to an excellent recent review by Liu and Jungnickel [1]. There is a degree of overlap of my review with that of Liu and Jungnickel, but the emphases are different. Between them, these two reviews offer a nice synthesis of the area.

2 Morphology

2.1 Crystallization in binary polymer blends

Let us first consider the case in which only one component (component A) of a melt-miscible polymer blend will crystallize, and that crystallization is in the form of spherulites. There are two limiting cases for the disposition of the noncrystallizing component B: either (1) B is totally excluded from the A-spherulites or (2) B is totally included within the spherulites. Between these two extremes lies a continuum of possibilities, with B being distributed partially within and partially outside the growing spherulites.

In fact, a very common case is that in which B is contained entirely, or nearly entirely, within the spherulites. In this case, microscopically, one finds one type of spherulite filling all space. The structural hierarchy within a spherulite is sketched in Figure 1. At the lowest level are stacks of thin, lamelliform crystal ribbons, separated from each other by uncrystallized polymers, as in Figure 1(c). The thickness of the crystals and the periodicity within the stack are typically of the order of 10 nm. Empirically, the number of crystals in a stack is limited, creating what has been termed fibrils or growth arms, as in Figure 1(b). The thickness of a fibril is typically of the order of 100–1000 nm. The noncrystallizing species B can be retained between crystalline lamellae or between fibrils of lamellae. An example of the retention of the noncrystallizing species between growth arms is shown in Figure 2 for a 50/50 syndiotactic/atactic polystyrene (sPS/aPS) blend crystallized isothermally at three different temperatures [2]. The noncrystalline aPS has been removed by washing with amyl acetate. Only the sPS growth arms remain; the voids are the loci of aPS within the spherulites. Note that the thickness of the growth arms and the interarm spacing both increase with increasing crystallization temperature.

A similar set of conditions exists for blends of two crystallizable melt-miscible polymers with significantly different melting points. Let A be the higher-melting component and B the lower-melting one. If isothermal crystallization of A is caused to occur between the melting points of the two polymers, then B cannot crystallize and will be separated into the interspherulite, interfibril or interlamellar space, just as for a component B which is incapable of crystallization. Upon further cooling, component B can also

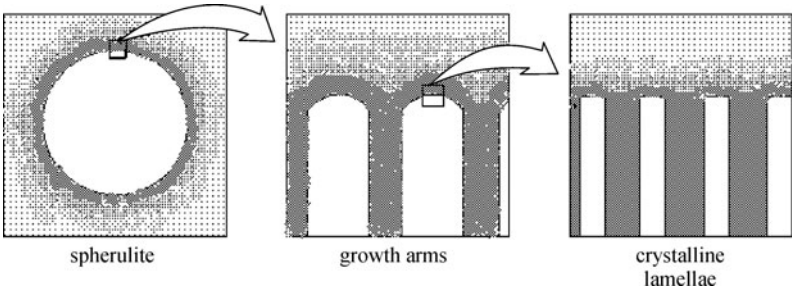

Figure 1 Structural hierarchy within a spheruite.

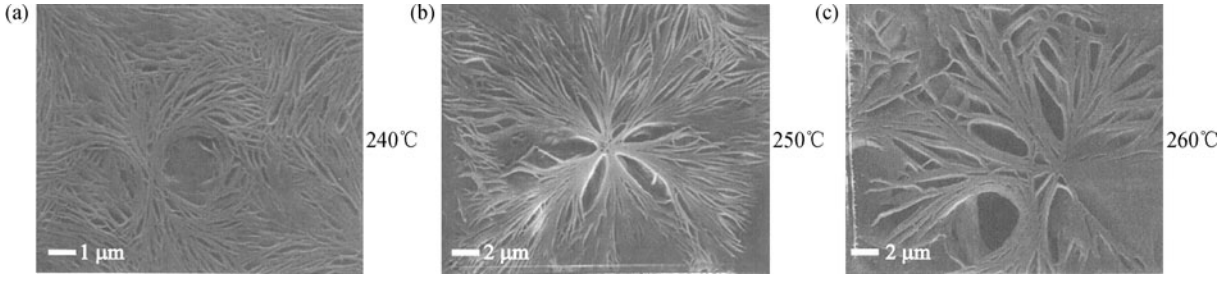

Figure 2 Scanning electron microscope images of an sPS/aPS 50/50 blend crystallized at different temperatures. aPS removed prior to microscopy. Figure reproduced from Ref. [2].

crystallize and its crystals will have been sequestered into one (or more) of the three possible locations. Examples of this behavior will be shown later.

That noncrystallizing or later-crystallizing species can exist between spherulites, fibrils or lamellar crystals has been known for some time (see Ref. [3]). While the location of polymer B between spherulites or growth arms can be directly observed by optical or electron microscopes, the fine scale of the interlamellar space makes the discovery of polymer B more difficult. Most often, small-angle X-ray scattering (SAXS) is used to probe this possibility. The presence of molecules of B between periodically stacked lamellae must increase the periodicity of those lamellae. The interlamellar periodicity produces a Bragg peak in SAXS, and from this peak the periodicity is measured. The same information can be obtained directly using electron microscopy. SAXS and electron microscopy investigations of polymer blends in which at least one component is crystallizable show that in some cases the interlamellar periodicity is significantly increased by the presence of the other component [4–13], and in some cases an increase in periodicity is either absent or weak [14–17]. The measurement of long periods using SAXS can be used to quantitatively assess the disposition of B between interlamellar and interfibrillar regions. To do so, the known overall concentration of B is used to compute what would be the increase in interlamellar spacing if all the B were concentrated there; comparing this value with the measured periodicity the difference between the overall concentration of B and the computed interlamellar concentration must be the portion contained between fibrils. As an example, Figure 3 shows the interlamellar periodicity (long period) of poly (ethylene oxide)/poly(vinyl acetate) (PEO/PVAc) blends as a function of PVAc content [11]. Shown is the experimental result and also what would be expected if all PVAc were to be present in the interlamellar space. Since the spherulites are also shown to be space-filling, most of the PVAc must reside between the growth arms, as this is the only remaining possibility.

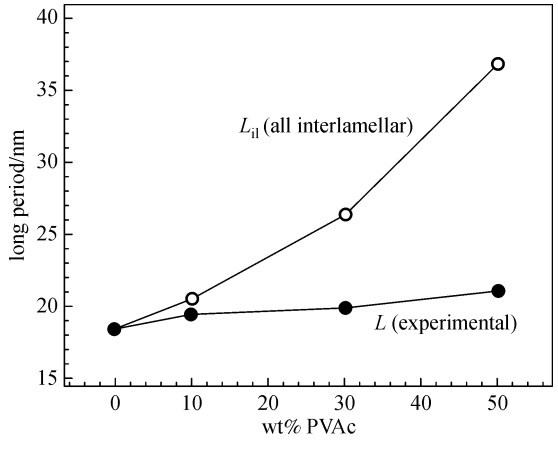

Figure 3 Experimental long periods (filled circles), along with the corresponding calculated values of L for all-interlamellar location of PVAc. Figure reproduced from Ref. [17].

Wang et al. [18] have directly observed the location of low-melting-point poly(butylene adipate) (PBA) crystal lamellae in higher-melting (and consequently first-formed) poly (butylene succinate) (PBS) spherulites. Depending on the concentrations of the components and on the crystallization temperature of the PBS spherulites, the PBA crystals can reside between PBS lamellae, between PBS growth arms, or between PBS spherulites. Figure 4 shows AFM phase contrast images of PBS/PBA 80/20 (a,b) and 20/80 (c,d) blends in which the PBS has been crystallized isothermally at 100°C and the PBA subsequently crystallized during continuous cooling. Figures 5(a) and 5(c) show the fully crystallized polymer at room temperature (PBA below its melting point), while Figs. 5(b) and 5(d) show the same areas and at 75°C (PBA molten). Features that are present at room temperature, but not at 75°C are then crystals of PBA. For the 80/20 blend the PBA lamellae (arrows) lie between PBS lamellae, while for the 20/80 blend the PBA lamellae are seen between the PBS growth arms. In this study, it is also reported that when the PBS is crystallized at 75°C the PBS spherulites fill the entire space, whereas when PBS is crystallized at 100°C PBS spherulites do not impinge, but are separated by PBA-rich material. Figure 5 shows, schematically, the effects of the blend composition and PBS crystallization temperature on the final morphology. Low crystallization temperatures and low PBA content favor interlamellar capture of PBA, while high crystallization temperatures favor interspherulitic placement. The interfibril location of PBA occurs at intermediate temperatures and PBA contents.

2.2 Simultaneous crystallization of two components in a polymer blend

We have just examined the morphology of solidified blends in which either only one polymer crystallizes or in which the melting points of the two crystallizable species are sufficiently disparate that the components crystallize sequentially. We now consider the case in which the two species crystallize isothermally at the same temperature, forming two distinct spherulite types. Nishi, Qiu, Ikehara and colleagues have reported on the morphology of a number of such systems [19–29]. A common theme through these reports is that, despite separate nucleation events, where possible, fibrils of the individual components tend to intermingle within spherulites.

Figure 6 is a polarized light micrograph of 50/50 poly (ethylene succinate)/poly(ethylene oxide) (PES/PEO) blend crystallizing at 47.5°C [29]. In (a) a rapidly growing PEO

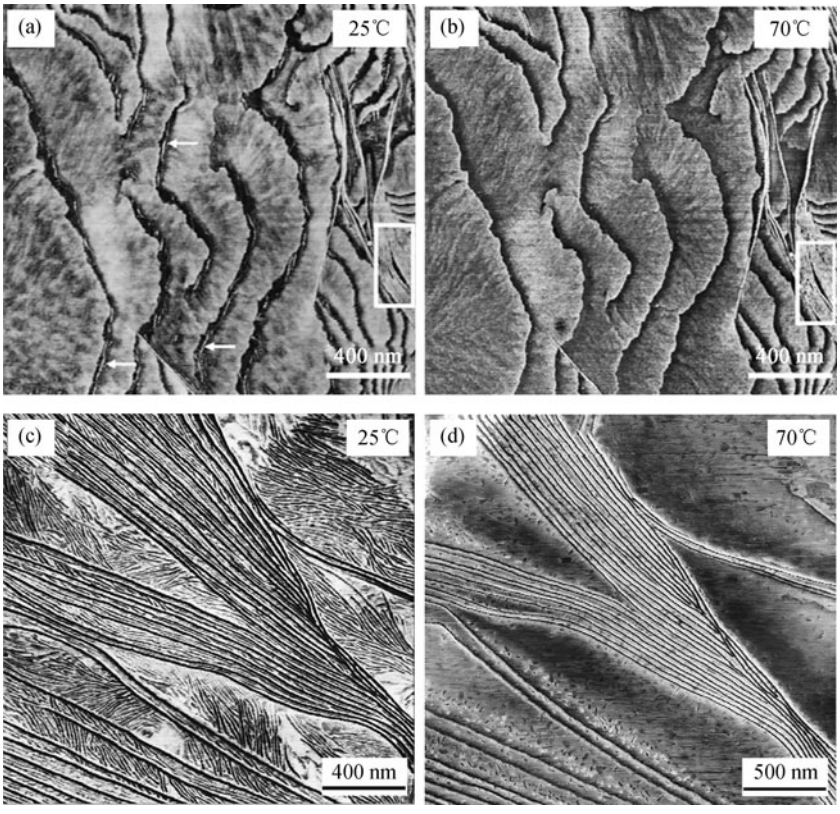

Figure 4 AFM phase images of (a), (b) 80/20 and (c), (d) 20/80 PBS/PBA blends, both with PBS first crystallized isothermally at 100°C and then continuously cooled to crystallize the PBA. The images were scanned at (a), (c) 25°C and (b), (d) 70°C. Figure reproduced from Ref. [18].

spherulite and a slower growing PES succinate spherulite are about to impinge. In (b) the growing spherulites are seen after impingement. There are two principal observations to be made in this micrograph and in others for this system. First, the birefringence in both spherulites is enhanced in the region near the impingement. This indicates that crystals of each component have grown into spherulites of the other *at the same orientation as the crystallites of the host spherulite*. Apparently the host templates the growth direction of the penetrating crystals. Second, the faster growing PEO has nucleated anew at the center of the PES spherulite and has grown through and beyond the growing PES spherulite. In the figure, the white arrows mark the PES spherulite and the black arrows mark the concentric PEO spherulite. (We will refer to these as *concentric spherulites*, although this is likely a misnomer.) So the PES spherulite has nucleated concentric spherulite-like growth of PEO crystals. Finally, it is found (not shown here) that the growth velocity of crystal lamellae of the penetrating species is greater than what it is in an isolated spherulite of the same component growing into the same melt. This effect is attributed to an increased concentration of the interpenetrating species within the spherulite of the other component. At a somewhat lower crystallization temperature, only concentric spherulites are found, as shown in Figure 7. Lu et al. have mapped the region of concentration-temperature space in which simultaneous spherulite growth (including concentric spherulites) is found [29].

An extreme case of directing the crystallization of a later crystallizing polymer by existing spherulites is seen in Figure 8. Figure 8 is a polarized optical micrograph of a 20/80 poly (butylene succinate)/poly(ethylene oxide) (PBS/PEO) blend crystallizing at 50°C [23]. Here the poly(butylene succinate) has already crystallized, with its spherulites filling the entire volume. The PEO is in the process of crystallizing. The PEO has begun crystallizing at the center of the bright circle, such that its growth perimeter is seen as the edge of the bright region. Beyond the bright region, smaller, poorly birefringent PBS spherulites fill the micrograph. As the PEO grows through the specimen, the birefringence of the PBS spherulites is enormously enhanced. Clearly the PEO crystals have become oriented in the same way as the host PBS crystals, thus enhancing the birefringence. As in the previous examples, the host spherulites act to direct and orient the growth of the component which crystallizes later.

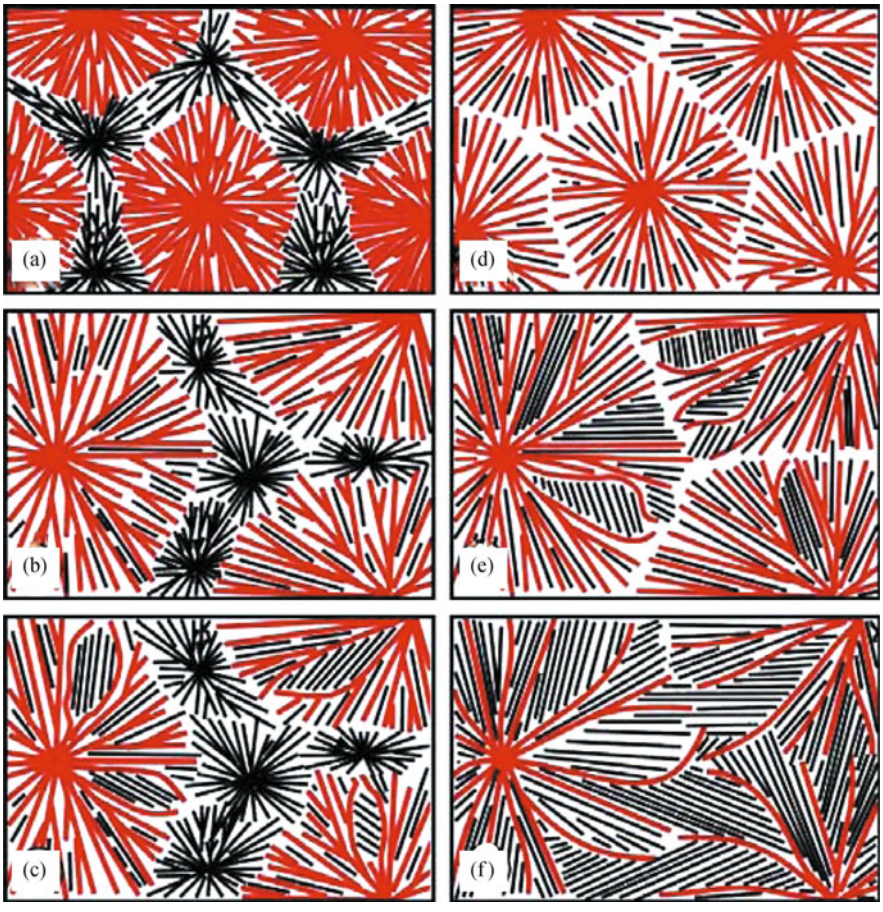

Figure 5 Sketches describing the phase segregation processes of different PBS/PBA blends at different temperatures. The red lines represent PBS, while the black ones represent the PBA crystals. Parts (a), (b), and (c) correspond to the crystallization of PBS at 100°C followed by quenching to low temperature for PBA crystallization, whereas parts (d), (e), and (f) are related to PBS crystallized at 75°C. Figure reproduced from Ref. [18].

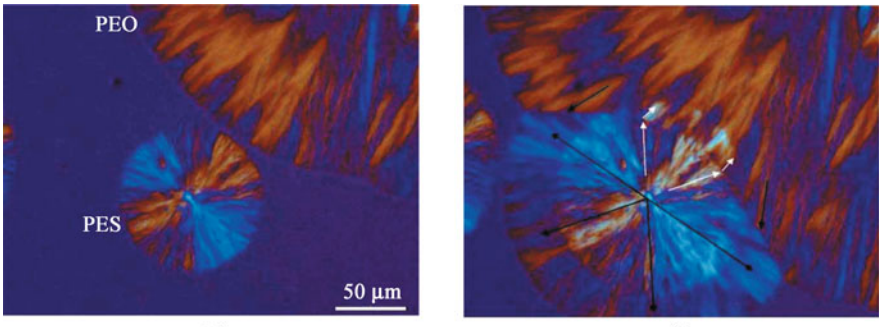

Figure 6 Spherulites of a blend of a 50/50 blend of PEO and PES crystallizing at 47.5°C: (a) before impingement and (b) after impingement. Figure reproduced from Ref. [29].

3 Kinetics of spherulite growth from miscible blends

3.1 Introduction

While the kinetics of spherulite growth might seem an arcane and perhaps tertiary aspect of the crystallization of crystalline blends, the actuality is that the simplest aspect of growth kinetics sheds considerable light on the fundamentals of this subject. The basic measurement in this case is the velocity of growth of the spherulite, and the most common finding is that the growth velocity is constant in time, although in some cases the growth velocity is $V \sim t^{-1/2}$ (the propagation of the

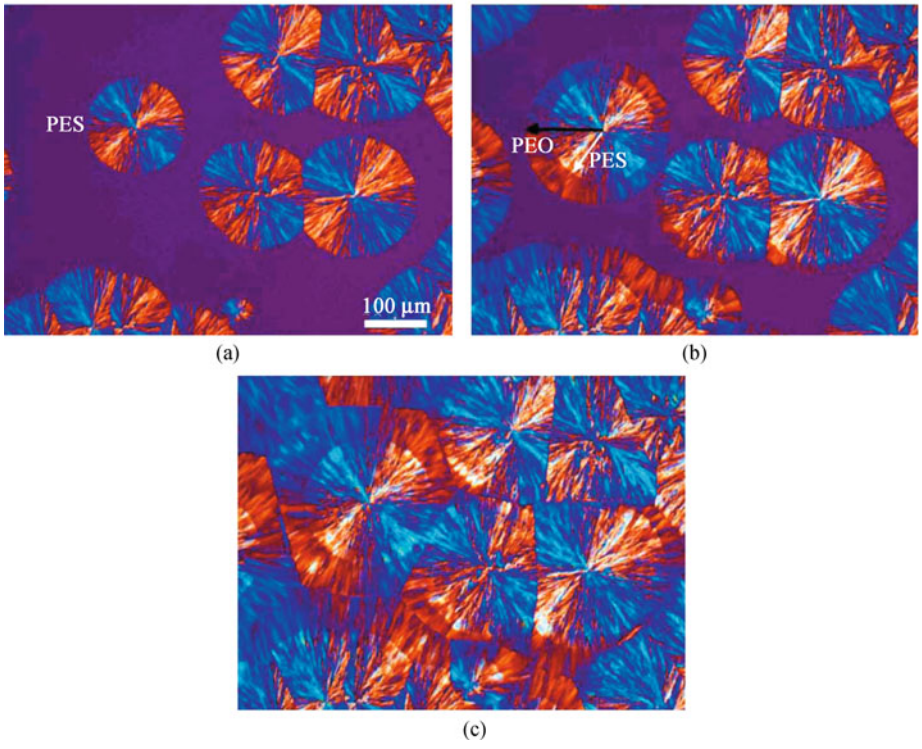

Figure 7 Polarized optical micrographs taken during the isothermal crystallization of a 50/50 PES/PEO blend at 42.5°C. Figure reproduced from Ref. [29].

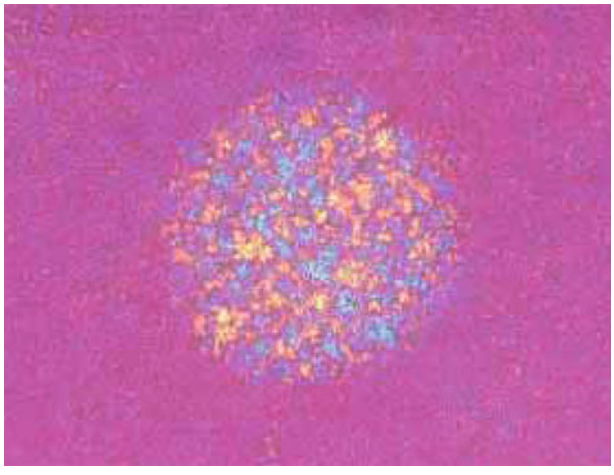

Figure 8 Polarized optical micrograph taken during isothermal crystallization of a 20/80 PBS/PEO blend at 50°C. Figure reproduced from Ref. [23].

spherulite radius is parabolic in time). Further, the same blend can show both constant and parabolic behavior, depending on the temperature, as shown for an 80/20 poly(butylene succinate)/poly(butylene acetate) (PBS/PBA) blend [18] in Figure 9.

3.2 Moving boundary problems

The implications of constant and parabolic growth velocities are best understood in terms of the results of moving boundary problems. Moving boundary problems are an area of the classical theory of diffusion [30]. In the present context, the problem can be considered as follows. In a binary polymer blend, it is exceedingly rare that both components crystallize in the same crystal (cocrystallization). Therefore as crystals of one component (A) grow into the binary melt, they must exclude molecules of the other component (B). As the crystal grows, the concentration of B builds up in the melt near the moving interface. If the "solute" cannot diffuse away from the interfacial region, it will continue to accumulate there and will choke the growth process. (It must be mentioned that the same condition can apply to heat, as well as to molecular concentration; the heat of fusion is liberated at the growth front and must also be conducted away. However, thermal conduction is seldom a problem in polymer crystallization [31].)

In the classical treatment of such a case (the Stefan problem), the growth front is allowed to propagate at exactly the rate which is consistent with the diffusion of B (or of the heat of fusion) away from the interface. The growth front

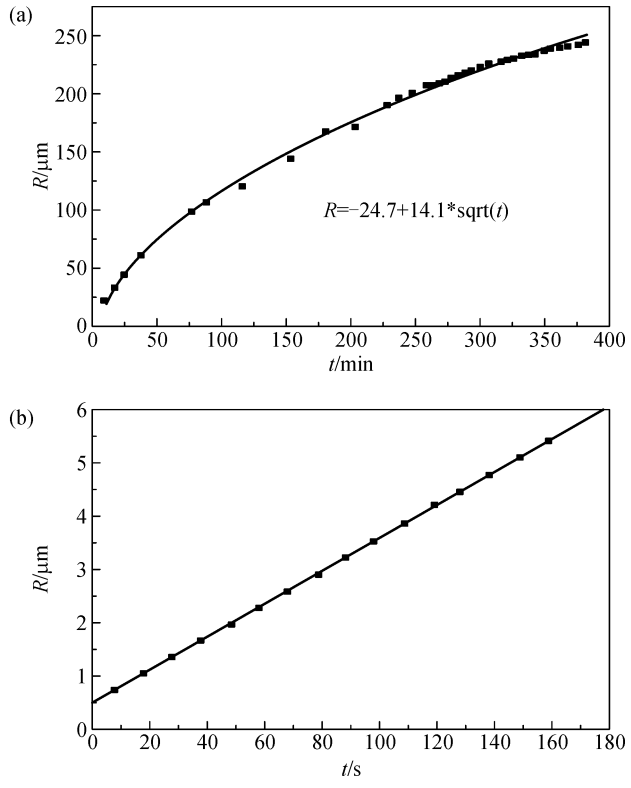

Figure 9 Radius of PBS spherulites versus crystallization time for PBS/PBA 80/20 blend crystallizing at (a) 100°C and (b) 75°C. Both temperatures are above the melting point of PBA (60°C). The line in (a) is the least squares parabolic fit and the line in (b) is the least squares linear fit. Figure reproduced from Ref. [18].

geometries which come immediately to mind are a sphere and a plane. These geometries imply one-dimensional diffusion of solute or heat from the growth front (normal to the spherical surface or to the plane). For these cases, no steady-state solution is found; the growth velocity cannot be constant in time. Rather, the growth front movement is parabolic, due to the continuous buildup of solute (or heat) in the melt near the interface.

In the case of a sphere or a plane, the solute builds up near the interface because it has nowhere to go except straight ahead, and that becomes increasingly difficult as more and more B is excluded from the growing object. This problem is relaxed in the case of the lengthwise growth of a needle or the lateral growth of a thin plate. In such cases, the diffusion can be normal to the growth direction, as well as in the growth direction. This is a much more efficient process than what is experienced for a planar or spherical front. Indeed, one can envision the B molecules as being "dumped" to the side, as opposed to having to be conveyed forward. For these cases a stationary solution is found; the growth velocity is constant. The growth velocity is, however, smaller than what it would be in the neat polymer. Solutions for plates and needles are reviewed by Christian [32].

With these general results in mind, we can begin to see what the experimental results for crystallization in polymer blends connote. If the growth velocity is parabolic in time, the spherulite grows as if it has a solid spherical front, and diffusion of the excluded molecules from the growth front is one-dimensional. In this case, the final result would be spherulites of polymer A fixed in a continuum of polymer B. If the growth velocity is constant in time, then growth occurs by the radial propagation of narrow growth arms (also known as "fibrils"). In this case, the noncrystallizing polymer would collect between the growth arms and the spherulites would (a) contain both polymer species and (b) fill all space. Morphologically, this is the more common case for polymer blends.

One additional aspect occurs if both polymer components are crystallizable. Suppose that the melting points of the two components are significantly different. If crystallization occurred at a temperature between the melting points of the two polymers, then the higher melting species (A) would crystallize, with the other species (B) acting as the uncrystallizable solvent. As the temperature is lowered further below the melting point of B, this component will also crystallize. Depending on whether B has been excluded from the growing A spherulites or included within them, the crystallized B will either form the continuum about the A spherulites or will crystallize within the original skeletal spherulites, forming composite crystalline spherulites.

4 The diffusion length and its implications

The solutions to moving boundary problems of alloys (blends), are in the form of the concentration c_B of B in the melt ahead of the growing interface. With the interface situated at $z = 0$, there is invariably contained in the c_B expression a factor $\exp\left(-\frac{V}{D}\right)z$, where V is the growth velocity, D is the mass diffusivity, and z is the distance from the interface into the melt. This factor – and indeed the concentration of B in the melt – falls to 1/e of its value at the interface at a distance $z^* = D/V$. This distance, normally represented by δ and called the *diffusion length*, is a measure of how far a typical molecule will diffuse during the propagation of the growth front.

Consider now Figure 1, which depicts the construction of a spherulite. The spherulite is composed of growth arms with a diameter and spacing of order 1 μm. The growth arms are in turn composed of ribbonlike crystals whose thickness is of the order 0.01 μm. The ribbons are stacked, separated by amorphous material. This amorphous layer also has a

thickness of the order 0.01 μm. Suppose that the diffusion length is quite small, of the order 0.01 μm. Then noncrystallizable B chains cannot move far, but can diffuse laterally, to fill the intercrystalline space. If the diffusion length is much larger than this, then the concentration fields of adjacent crystals overlap, and the concentration field begins to look like that of a solid front. In this case, one would expect a parabolic growth velocity. However, since the crystal ribbons are collected into growth arms, there is the new opportunity for B to diffuse laterally to the space between the growth arms, until the diffusion length becomes significantly greater than the interarm spacing (ca. 1 μm). Beyond this magnitude of the diffusion length, the concentration fields of the growth arms significantly overlap, and the system acts as a solid spherulite, excluding solute from itself and exhibiting parabolic growth kinetics.

5 Simulations of the effects of diffusion length on morphology

The diffusion length is given by D/V. V has a very much stronger dependence on temperature than has D (although the temperature dependence of the diffusivity is itself very strong). The diffusion length can thus be controlled via the temperature of crystallization, the diffusion length increasing with increasing crystallization temperature. Kit has simulated the crystallization of a blend of crystallizable syndiotactic and noncrystallizable atactic polystyrene, using a finite element model of the growth front [2,33]. The model is sketched in Figure 10. At the left is sketched a stack of thin ribbonlike crystals spawned by a giant screw dislocation [34] (not shown) in the longest (first generated) ribbon. The crystals are spawned at intervals Δt. The computational cell is shown at the right. Seen is one-half of a stack of ribbonlike crystals growing into a melt, beginning (bottom) with half of the original ribbon. Here, two new ribbons have been spawned. At each interment of time Δt a new crystal is spawned and the diffusion equations are solved, to obtain the composition at each position in the melt. It is assumed that the growth velocity of each ribbon is slowed by the dilution $(1 - c_B)$ of crystallizable polymer in the melt at the growth front, where c_B is the concentration of uncrystallizable material. This represents the simplest physics for a concentration effect. In the next Δt step, each ribbon moves forward an amount dictated by its concentration-restricted velocity. In Figure 11 is shown the simulated growth fronts after 20, 40, 60, 80, and 100 steps, using parameters for a 50/50 syndiotactic/atactic polystyrene blend system [2]. We see that the first few lamellae grow much faster than the remainder. These initial crystals are able to dissipate the rejected component B laterally, where it collects above the later-formed ribbons. The fast growing crystals grow at a constant velocity (you can check this by looking at the positions of the initial crystal after 20, 50, 60, 80, 100 steps), whereas the growth kinetics of the crystals farther from this growth arm turns out to be parabolic. The expectation for a blend system is that the growth arm thickness should increase with diffusion length, and hence with temperature, since the uncrystallizable B molecules can diffuse laterally farther. This is found to be the case, both experimentally and, in Kit's simulation, with a reasonable fit of predicted and measured arm thicknesses. The effect of crystallization temperature on arm thickness can be seen in the micrographs of Figure 1.

We would likewise expect that the growth arm spacing should increase with diffusion length and crystallization temperature. This is known experimentally and has been predicted analytically by Balijepalli [35]. Balijepalli modified Zener's classical analysis of eutectoid solidification [36] to represent growth of spherulites of polymer A from an A/B blend. In the eutectoid case, A-rich α crystals and B-rich β

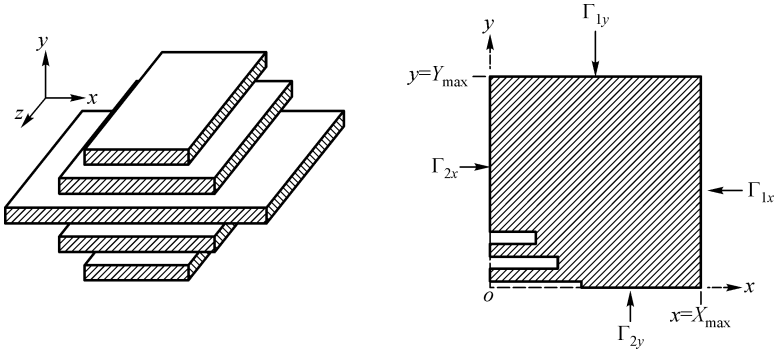

Figure 10 Left, the conceptual model [2,33]: a new crystal lamella, growing in the x-direction, is spawned at the top of the stack every time interval Δt. Right, the computational cell, showing one-half of the initial lamella and two spawned lamellae. The diffusion equations are solved each time interval Δt, and the new concentrations used to compute lamella propagation i the next time interval. Figure reproduced from Ref. [2].

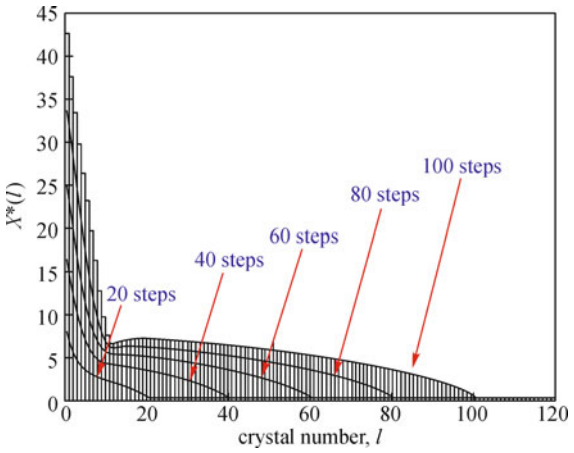

Figure 11 Results of the finite element simulation described in Figure 10 [2]. Each solid line shows the length of each lamella after the given number of steps, ending with 100 steps.

crystals must evolve from a mixed A/B solid. A very small diffusion length dictates that thin α and β crystals platelets grow side-by-side, so that molecular diffusion need occur only over a lateral distance of essentially one crystal's thickness. This system is sketched in Figure 12 and is similar to the situation for crystallization in polymer blends; in both cases the components have to redistribute at the growth front. As one might expect from the temperature-dependence of the diffusion length, the periodicity of stacking becomes larger and larger with increasing transformation temperature. Balijepalli's analysis predicts arm spacings and growth velocities nicely for higher diffusion lengths, but departs from agreement at lower diffusion lengths (due largely to an approximation made in the analysis) [35].

At sufficiently small diffusion lengths, the morphology at the interlamellar level should be affected. We know empirically that the crystal thickness is specified only by the crystallization temperature. If individual crystal lamellae were to exclude noncrystallizable species B laterally as they grow, then the interlamellar separation should grow markedly with the concentration of B. Such increased separation of lamellae would have two effects: (1) the concentration fields of B would overlap less and (2) overall transformation of melt to crystal would decrease, since the relative volume transformed decreases. The first-named effect would increase the crystallization rate of each lamella, as the concentration of B at the growth front would be reduced relative to its value if the spacing had not increased. However, the second effect could be more important. Consider the extreme case in which the interlamellar space approaches infinity. The overall transformation of melt to crystal would then approach zero. Now let us presume that the operating principle chosen by nature is the maximum rate of transformation of melt to crystal (fastest decrease in free energy). Kit has simulated the crystallization of lamellar stacks, again using a finite elements analysis [37], seeking the inter lamellar spacing l_a that provides the maximum overall transformation rate at given conditions of diffusion length and blend composition. He found that blend systems separate into two types of behavior: systems with small diffusion lengths show minimal increase in interlamellar spacing, whereas systems with larger diffusion lengths show substantial increase in lamellar spacing. He further found that the behavior of a wide range of blend systems demonstrates this behavior. We can understand this as follows. At very small diffusion lengths, $\delta < l_c$ (where l_c is the lamellar thickness), molecules of neither components A nor B move more than l_c, and the interlamellar space can vary only from its value in the absence of blending to a value about δ larger. However, as δ becomes significantly larger than l_c, the interlamellar space can grow very large, limited only by the condition that the overall transformation rate be maximized. Figure 13 shows the results for normalized interlamellar space

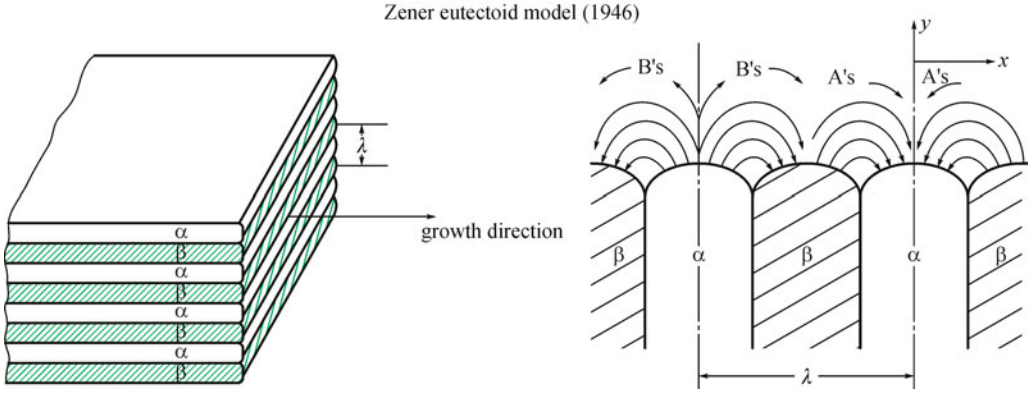

Figure 12 The Zener eutectoid model [36]. Stacks of thin lamellar crystals of A-rich α and B-rich β are formed in order to maximize the growth velocity by minimizing the distance that A molecules rejected by β crystals and B molecules rejected by α need move to reach the growth fronts of α and β crystals, respectively.

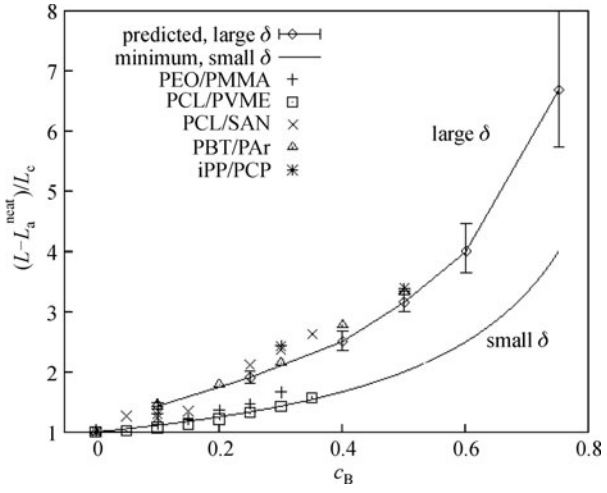

Figure 13 Measured and predicted values of the normalized long spacing. The two lines represent the simulated results for small and large diffusion lengths. In the normalization, L is the stacking periodicity (the long spacing), L_a^{neat} is the thickness of the amorphous layer for the neat (unblended) polymer and L_c is the crystal thickness. c_B is the volume fraction of B. Figure reproduced from Ref. [37].

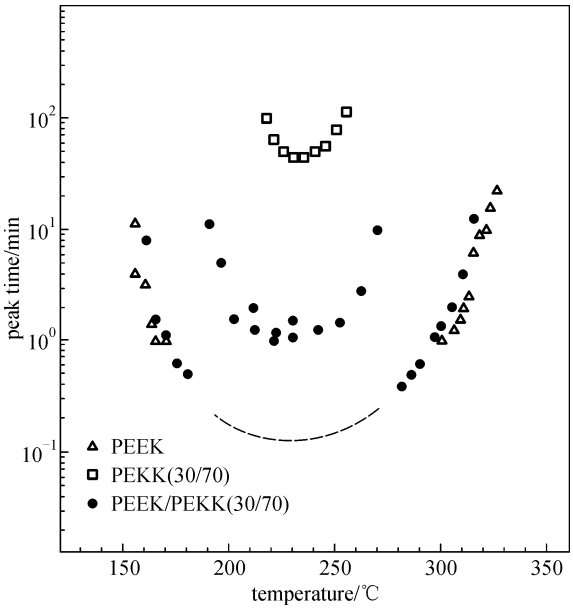

Figure 14 Peak crystallization time versus temperature for neat PEEK, PEEK(30/70) and a 50/50 blend of the two. Figure reproduced from Ref. [38].

versus concentration of B for several systems. Shown also are Kit's simulated results [37] for small and large values of the diffusion length normalized by the lamellar thickness (values of δ still smaller than growth arm dimensions). The agreement of theory and prediction is very good.

6 Synergistic kinetics

Figure 14 illustrates an interesting kinetic effect which has been observed in several blend systems in which the components are rather similar. In this case differential scanning calorimetry has been performed during isothermal crystallization of poly(ether ether ketone) (PEEK), poly(ether ketone ketone)30/70[1)] (PEKK(30/70)), and a 50/50 blend of these two polymers [38]. The time to reach the exothermic crystallization peak (or peaks) has been plotted against crystallization temperature for all three materials. In the figure it is seen that PEEK crystallizes very rapidly, some 2–3 orders of magnitude faster than PEKK(30/70) at all temperatures. (Between 180°C and 260°C PEEK crystallizes too rapidly for its kinetics to be captured.) However, over a span of temperatures where the PEEK kinetics are most rapid, the blend crystallizes with the kinetics between those of the two neat polymers. In Figure 14, each plotted data point represents an exothermic crystallization peak. For the PEEK/PEKK(30/70) blend, as seen in the figure, sometimes there is only one exotherm (one data point at that temperature) and sometimes there are two closely spaced exotherms (two points at the temperature). Clearly there is some form of cooperation between the crystallization processes of the component polymers. Consequently, this phenomenon has been called *cooperative crystallization*. This kind of behavior has been reported in a several systems [11,39–42]. The PEEK/PEKK (30/70) result is the most extreme case heretofore reported; other examples operate similarly, but with less dramatic kinetic differences.

It is easy to qualitatively understand how the kinetics of the more rapidly crystallizing polymer might be slowed by the necessity to redistribute the component polymers in the melt near the growth front. It is less easy to understand or determine how the kinetics of the slower crystallizing species can be increased by more than an order of magnitude. There are several possibilities for how the kinetics of the slower crystallization could be affected, as follows:

(1) Enhanced nucleation at the center of concentric spherulites. This phenomenon has been directly seen in one cooperatively crystallizing system, PES/PEO, by He and Liu [42]. They observed that in this system cooperative crystallization (they use another term) occurs only when crystallization of the slower crystallizing species nucleates at the center of a growing spherulite of the more rapidly crystallizing species (concentric spherulites).

(2) Enhanced nucleation throughout growing spherulites of the faster crystallizing component. While there is no direct

0) PEKK(30/70) is a random copolymer containing 30% terephthalic ether ketone ketone linkages amd 70% isopthalic linkages..

evidence for this within blend spherulites, it must be considered likely. Either of two mechanisms could be operative here. It is possible that crystals of component B epitaxially nucleate on existing lamellar crystals of A. A second mechanism would be alignment of chains of B in the melt near the surface of existing crystals of A. This phenomenon has been demonstrated for thin molten films above existing polymer crystals [43,44], but its role within blend spherulites is not known.

(3) Enhanced growth velocity due to removal of component A. The uncrystallized material within a spherulite of the more rapidly growing component A must be richer in B than is the original melt, since A has been removed to form the spherulite. Effects of dilution of A, of increased supercooling of B, and, sometimes, of removal of more viscous component A on the subsequent crystallization of B should thus increase both the rates of nucleation and growth of B, relative to their kinetics in the original melt. Increased growth velocities within growing or existing spherulites, relative to the velocities in free-growing B spherulites in the same blend, have been documented by Lu et al. [29]. There is, however, no way that these effects could increase the growth velocity relative to what it is in neat polymer B.

7 Crystallization in blends with an UCST or an LCST

Polymer blends often exhibit miscibility gaps. Schematic phase diagrams of systems having (a) a lower critical solution temperature (LCST) or (b) an upper critical solution temperature (UCST) are shown in Figure 15. In both cases, the area under the arc is a region of liquid phase separation. For such systems it is possible for liquid-liquid phase separation (LLPS) to compete with crystallization, providing still further morphological and property variations. Given the rich possibilities in such systems, they are surprisingly sparsely investigated.

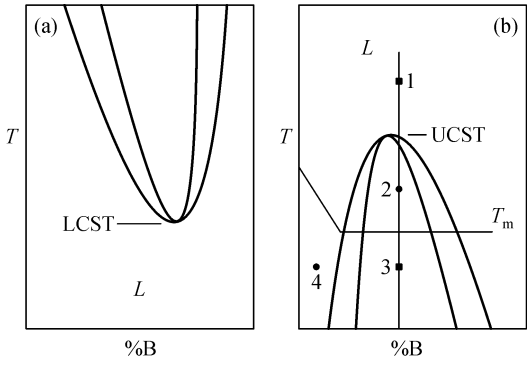

Figure 15 Schematic polymer binary phase diagrams, showing systems with (a) a lower critical solution temperature (LCST) and (b) an upper critical solution temperature (UCST). In both cases, the area under the arc is a region of liquid-liquid phase separation. For reference within this section, a melting point line (T_m) and points 1–4 are indicated in (b).

The possibilities of engineering morphologies within UCST systems are large. For UCST systems with one crystallizable component, it is frequently found that the melting point of the crystallizable polymer lies at a temperature within the temperature range of the miscibility gap, as indicated in Figure 15(b). For such systems, the thermal schedule for solidification can be important in defining the microstructure. Consider the composition indicated by the thin vertical line in the figure, and let the material be molten in the homogeneous liquid at position 1. From there, the material could be quenched to position 3, below the melting point of the crystallizable polymer A. At this temperature the kinetics of LLPS can compete with those of crystallization. Most often, crystallization is faster. We shall look at this possibility in the following paragraph. Another possibility is to quench from temperature 1 to temperature 2, and later to temperature 3. This two-step treatment allows some degree of LLPS to occur before crystallizing at point 3. Finally, one could have a composition and temperature outside the phase-separated arc, but also below T_m, as indicated by point 4. We now consider these three possibilities.

As mentioned above, within a miscibility gap the rate of crystallization is frequently faster than the rate of liquid-liquid phase separation. In this case, when the blend is quenched from 1 to 3 in Figure 15(b), spherulites of crystallizable polymer A will form first, followed by phase separation of the remaining melt (which is now rich in B). Figure 16, taken from Tanaka and Nishi [45], shows the morphology of one such system. This is a 40/60 blend of crystallizable poly (caprolactone) (PCL) and uncrystallizable atactic polystyrene (aPS) crystallized at 25°C. Figure 16(a) is an optical microscope image taken under crossed polarizers. The contrast under crossed polarizers derives from optical birefringence. In a system with no orientation in the amorphous phase, only crystals can contribute to the contrast. Thus, in Figure 16(a) we see only the PCL spherulites. Figure 16(b) is the same area taken under conditions of phase contrast. Phase contrast is sensitive to the interfaces between regions of different indexes of refraction. In this case, the boundaries between the phase-separated liquid regions will be seen, as well as crystal-amorphous boundaries. In this micrograph one sees the weak images of the spherulites, with the LLPS regions appearing as a more strongly contrasted fine structure within the spherulites. The PCL spherulites have formed with aPS-rich liquid between the growth arms (or, possibly, lamellae), and these liquid pockets have subsequently phase-separated.

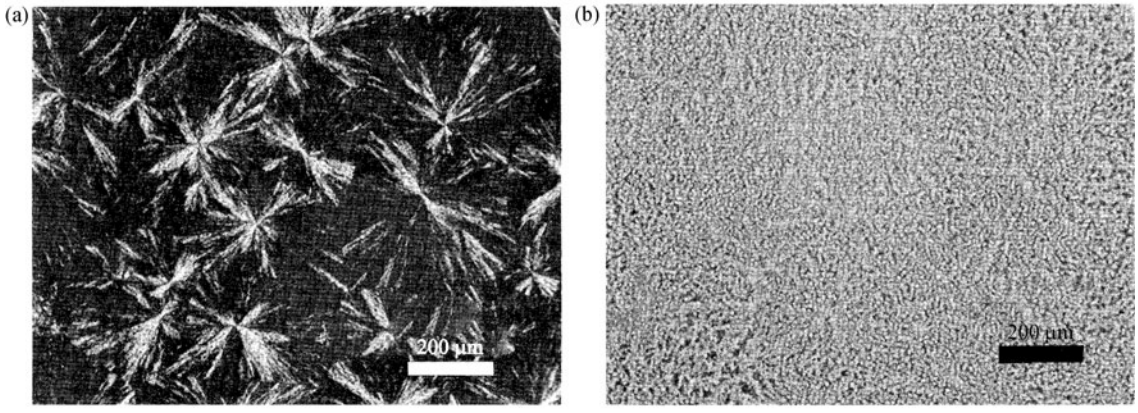

Figure 16 Optical micrographs, at room temperature, of a 40/60 PCL/aPS blend which was quenched from the homogeneous liquid to a temperature below the melting point of PCL. (a) is taken under crossed polarizers. (b) is the same area taken under phase contrast. Figure reproduced from Ref. [45].

Wang, Han and coworkers have studied the effects of partial LLPS [46–51] on the morphology of polyolefin blend systems with a UCST. This is the path 1 → 2 → 3 in Figure 15(b). Figure 17(a) shows the phase diagram of one of the blend systems they have studied, poly(ethylene-co-hexene)/poly(ethylene-co-butene) (PEH/PEB). In this system, only PEH can crystallize. The line derived from the triangles is the melting point of PEH in this system. They report for a 40/60

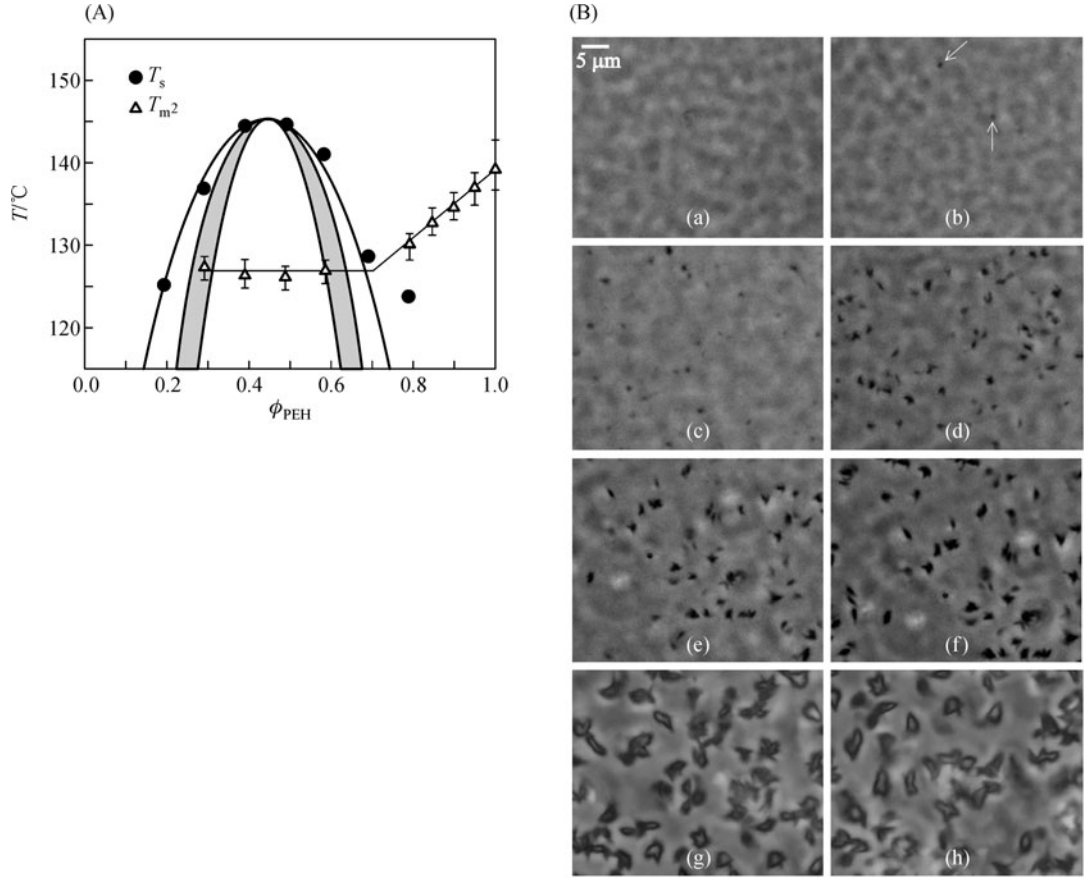

Figure 17 (A) Phase diagram of the PEH/PEB system, including the melting point of PEH (triangles). (B) Phase contrast optical micrographs of a PEH/PEB = 40/60 sample: (a) LLPS at 135°C for 20 h, (b) then isothermally crystallized at 125°C for 32, (c) 55, (d) 92, (e) 114, (f) 135, (g) 367, and (h) 486 min. Figure reproduced from Ref. [49].

blend the effect of LLPS time at 135°C on subsequent crystallization at 125°C. Figure 17(b) shows phase contrast optical micrographs taken at different times during crystallization of PBH. The crystallized areas appear black against the mottled gray-white phase-separated background. Analyzing such micrographs, they find that nucleation is induced at locations of the steepest concentration gradient during the spinodal LLPS. The effect of increasing the LLPS time is always to decrease the nucleation rate R (and thereby to refine the spherulite size), as shown in Figure 18 [49].

Tanaka and Nishi have reported on a crystallization process beginning outside the miscibility gap (point 4 in Figure 15(b), using a blend of crystallizable poly(caprolactone) (PCL) and uncrystallizable atactic polystyrene (aPS) [45,52]. An optical micrograph of a growing spherulite in a 70/30 PCL/aPS is shown in Figure 19(a). At the perimeter of the spherulite are droplets of an aPS-rich liquid. (These droplets will later elongate in the radial direction and be encompassed by the growing spherulite.) Figure 19(b) is a schematic phase diagram showing the sequence of events leading to the morphological result of Figure 19(a). The 70/30 blend is taken to the temperature T_i, where it is a molecularly mixed melt. Subsequently, the specimen is quenched to T_c, below the melting point of PCL and held there as the PCL crystallizes. The kinetics of spherulite growth are parabolic, indicating that the aPS is rejected from the spherulite. As the spherulite grows, the surrounding melt then becomes richer in aPS, moving the adjacent liquid toward and finally into the two-phase region of the phase diagram. The melt closest to the growth front would have the highest aPS concentration and liquid-liquid phase separation must occur there: the observed droplets.

There are few reports on crystallization from blends having a lower critical solution temperature. Inaba et al. [53,54] and Svoboda et al. [55] have investigated blends in which the melting point lies significantly below the phase separated region of the phase diagram. Using blends of crystallizable isotactic polypropylene (iPP) and noncrystallizable ethylene-propylene random copolymer (EPR), Inaba et al. first held the blends above the UCST and subsequently crystallized the iPP below its melting point (below the miscibility gap). They found that the final morphology could be either LLPS domains within iPP spherulites or iPP spherulites within iPP-rich LLPS domains, depending on the crystal nucleation rate of iPP. Svoboda et al. studied the effect of time of phase separation on the subsequent crystallization of PCL in PCL/SAN blends. They found that PCL crystallized slowly in the blend, but increased in rate with increasing LLPS time, an effect of increasing the PCL concentration in the PCL-rich phase.

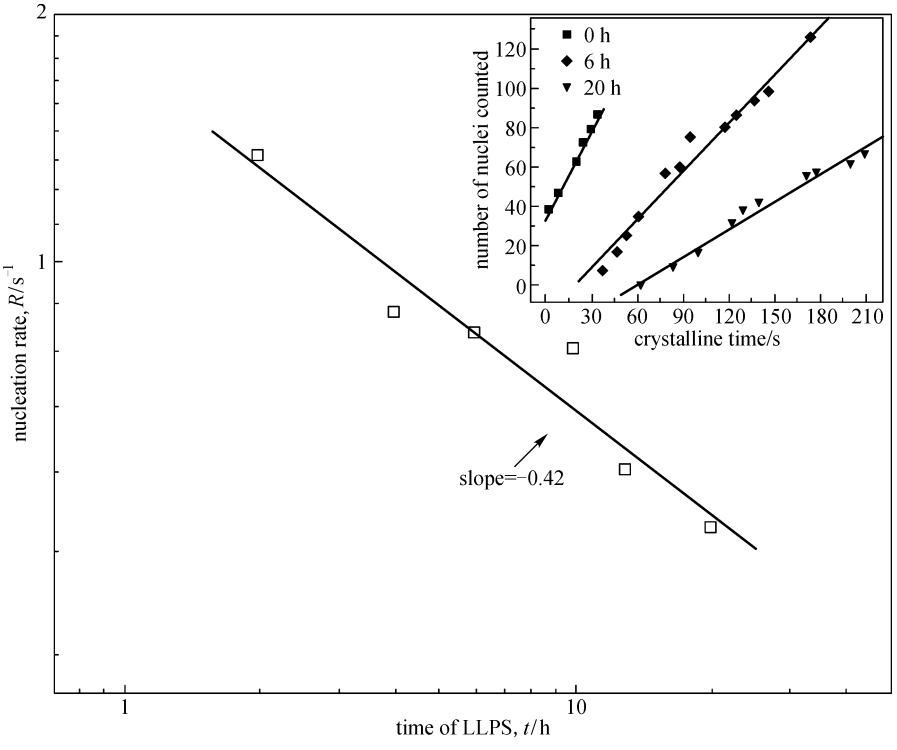

Figure 18 Log-log plot of spherulite nucleation rate R against LLPS time for PEH/PEB = 40/60 at 117°C after LLPS at 135°C. Inset shows time evolution of the number of nuclei for the PEH/PEB = 40/60 sample at 117°C after LLPS at 135°C for 0, 6, and 20 h, respectively. Figure reproduced from Ref. [49].

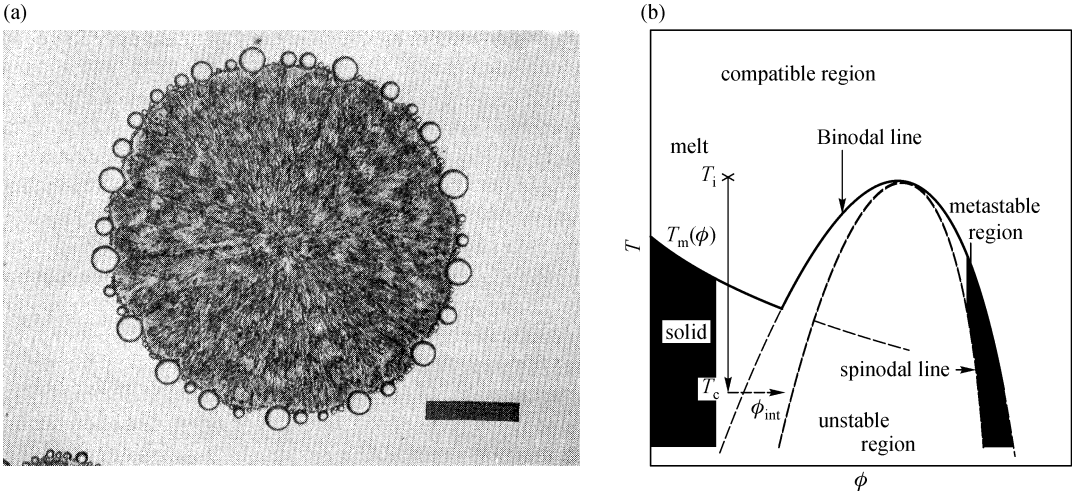

Figure 19 Crystallization of a 70/30 PCL/aPS blend at 50.0°C. (a) optical micrograph made during crystallization of a PCL spherulite. (b) schematic phase diagram indicating the process, beginning with a quench from a homogeneous melt at T_i, followed by crystallization at T_c. During crystallization, the concentration of aPS in the adjacent melt moves to the right, finally ending in the miscibility gap. Figures reproduced from (a) Ref. [45] and (b) Ref. [52].

8 Summary

During crystallization from a homogeneous melt, the components of a binary blend must redistribute themselves during the crystallization, since cocrystallization is rare. In the case that one component (A) crystallizes first, the other component (B, which may be either uncrystallizable or crystallizable but prevented from crystallization at this temperature) will be excluded and will finally locate between spherulites of A, between growth arms of A within the spherulite, or between crystalline lamellae of A within the spherulite. Which of these sites is chosen depends on the diffusion length of the system, itself a strong function of temperature. Models of the crystallization behavior give satisfactory agreement with observation.

When both components crystallize concurrently or nearly concurrently, additional phenomena can be observed: the development of interpenetrating spherulites and concentric spherulites, and cooperative crystallization, in which the kinetics of the components are matched. Our understanding of these features is as yet not well developed.

When there is the possibility of either liquid-liquid phase separation or crystallization, these processes can be caused to compete in controlled ways, creating a large variety of morphologies. Such systems require considerably more investigation than they have been given heretofore.

References

1. Liu, J.; Jungnickel, B. J., *J. Polym. Sci., Polym. Sci. Ed.*, **2007**, *45*, 1917–1931
2. Kit, K. M.; Schultz, J. M., *J. Polym. Sci., Polym. Phys. Ed*. **1998**, *36*, 873–888
3. Stein, R. S.; Khambatta, F. B.; Warner, F. P.; Russell, T.; Escala, A.; Balizer, E. *J. Polym. Sci., Polym. Symp*. **1978**, *63*, 313–328
4. Khambatta, F. B.; Russell, T.; Warner, F.; Stein, R. S., *J. Polym. Sci., Polym. Phys. Ed*. **1976**, *14*, 1391
5. Russell, T. P.; Stein, R. S., *J. Polym. Sci., Polym. Phys. Ed*. **1983**, *21*, 999–1010
6. Martuscelli, E.; Demma, G.; Rossi, E.; Segre, A. L., *Polymer* **1984**, *25*, 1097–1106
7. Russell, T. P.; Ito, H.; Wignall, G. D., *Macromolecules* **1988**, *21*, 1703–1709
8. Martuscelli, E.; Canetti, M.; Seves, A., *Polymer* **1989**, *30*, 304–310
9. Defieuw, G.; Groeninckx, G.; Reynaers, H., *Polymer* **1989**, *30*, 2158–2163
10. Defieuw, G.; Groeninckx, G.; Reynaers, H., *Polymer* **1989**, *30*, 2164–2169
11. Runt, J. P.; Zhang, X.; Miley, D. M.; Gallagher, K. P.; Zhang, A., *Macromolecules* **1992**, *25*, 3902–3905
12. Yang, F.; Qiu, Z.; Yang, W., *Polymer* **2009**, *50*, 2328–2333
13. Vaughan, A. S., *Polymer* **1992**, *33*, 2513–2521
14. Oudhuis, A. A. C. M.; Thiewes, H. J.; van Hutten, P. F.; ten Brinke, G., *Polymer* **1994**, *35*, 3936–3942
15. Talibuddin, S.; Wu, L.; Runt, J.; Lin, J. S., *Macromolecules* **1996**, *29*, 7527–7535
16. Wang, W.; Schultz, J. M.; Hsiao, B. S., *Macromolecules* **1997**, *30*, 4544–4550
17. Fragiadakis, D.; Dou, S.; Colby, R. H.; Runt, J., *Macromolecules* **2009**, *42*, 6581–6587
18. Wang, H.; Gan, Z.; Schultz, J. M.; Yan, S., *Polymer* **2008**, *49*, 2342–2353
19. Ikehara, T.; Nishi, T., *Polym. J*. **2000**, *32*, 683–687

20. Hirano, S.; Terada, Y.; Ikehara, T.; Nishi, T., *Polym. J.* **2001**, *33*, 371–373
21. Qiu, Z.; Ikehara, T.; Nishi, T., *Macromolecules* **2002**, *35*, 8251–8254
22. Ikehara, T.; Nishikawa, Y.; Nishi, T., *Polymer* **2003**, *44*, 6657–6661
23. Qiu, Z.; Ikehara, T.; Nishi, T., *Polymer* **2003**, *44*, 2799–2806
24. Ikehara, T.; Kimura, H.; Qiu, Z., *Macromolecules* **2005**, *38*, 5104–5108
25. Ikehara, T.; Kurihara, H.; Qiu, Z.; Nishi, T., *Macromolecules* **2007**, *40*, 8726–8730
26. Qiu, Z.; Yan, C.; Lu, J.; Yang, W., Ikehara, T.; Nishi, T., *J. Phys. Chem. B* **2007**, *111*, 2783–2789
27. Ikehara, T.; Jinnai, H.; Kaneko, T.; Nishioka, H.; Nishi, T., *J. Polym. Sci., Polym. Phys. Ed*. **2007**, *45*, 1122–1125
28. Qiu, Z.; Yan, C.; Lu, J.; Yang, W., *Macromolecules* **2007**, *40*, 5047–5053
29. Lu, J.; Qiu, Z.; Yang, W., *Macromolecules* **2008**, *41*, 141–148
30. H. S. Carslaw and J. C. Jaeger, *Conduction of Heat in Solids*, Oxford University Press: Oxford, UK, 1959, Chapter XI
31. Schultz, J. M., *Polymer Crystallization*, Oxford University Press: New York, 2001, p 209
32. Christian, J. W., *The Theory of Transformations in Metals and Alloys*, Pergamon Press: Oxford, UK, 1965, p 562–566
33. Kit, K. M.; Schultz, J. M., *Int. J. Numer. Methods Eng*. **1997**, *40*, 2679–2692
34. Geil, P. H., *Polymer Single Crystals*, John Wiley: New York, 1963, p. 153–163, 212–215, 291–298
35. Balijepalli, S.; Schultz, J. M., *Macromolecules* **2006**, *39*, 7407–7414
36. Zener, C., *AIME Trans*. **1946**, *167*, 550
37. Kit, K. M.; Schultz, J. M., *Macromolecules* **2002**, *35*, 9819–9824
38. Wang, W.; Schultz, J. M.; Hsiao, B. S., *Macromolecules* **1997**, *30*, 4544–4550
39. Hsiao, B. S.; Gardner, K. H.; Schultz, J. M.; Wang, W., *SPE/ ANTEC '93, Proceedings of the 51st Annual Technical Conference*, 1993, 1004–1009
40. Evstatiev, M.; Schultz, J. M.; Petrovich, S.; Georgiev, G.; Fakirov, S.; Friedrich, K., *J. Appl. Polym. Sci*. **1998**, *67*, 723–737
41. Balijepalli, S.; Schultz, J. M.; Lin, J. S., *Macromolecules* **1996**, *29*, 6601–6611
42. He, S.; Liu, J., *Polym. J*. **2007**, *39*, 537–542
43. Zhang, Y.; Lu, Y.; Yan, S.; Shen, D., *Polym. J*. **2005**, *37*, 133–136
44. Yan, C.; Li, H.; Zhang, J.; Ozaki, Y.; Shen, D.; Yan, D.; Shi, A. C.; Yan, S., *Macromolecules* **2006**, *39*, 8041–8048
45. Tanaka, H.; Nishi, T., *Phys. Rev. Lett*. **1985**, *55*, 1102–1105
46. Wang, H.; Shimizu, K.; Kim, H.; Hobbie, E. K.; Wang, Z. G.; Han, C. C., *J. Chem. Phys*. **2002**, *116*, 7311
47. Matsuba, G.; Shimizu, K.; Wang, H.; Wang, Z.; Han, C. C., *Polymer* **2004**, *45*, 5137–5144
48. Zhang, X.; Wang, Z.; Muthukumar, M.; Han, C. C., *Macromol. Rapid Commun*. **2005**, *26*, 1285–1288
49. Zhang, X.; Wang, Z.; Dong, X.; Wang, D.; Han, C. C., *J. Chem. Phys*. **2006**, *125*, 24907–24915
50. Zhang, X. H.; Wang, Z. G.; Zhang, R. Y.; Han, C. C., *Macromolecules* **2006**, *39*, 9285–9290
51. Zhang, X.; Wang, Z.; Han, C. C., *Macromolecules* **2006**, *39*, 7441–7445
52. Tanaka, H.; Nishi, T., *Phys. Rev. A* **1989**, *39*, 783–794
53. Inaba, N.; Sato, K.; Suzuki, S.; Hashimoto, T., *Macromolecules* **1986**, *19*, 1690–1695
54. Inaba, N.; Yamada, T.; Suzuki, S.; Hashimoto, T., *Macromolecules* **1988**, *21*, 407–414
55. Svoboda, P.; Kressler, J.; Inoue, T., *J. Macromol. Sci. Part B Phys*. **1996**, *35*, 505–525